

Carleton College

Carleton Digital Commons

Faculty Work

Physics and Astronomy

2005

Discovery of pulsed OH emission stimulated by a pulsar

Joel M. Weisberg

Carleton College

Simon Johnston

University of Sydney, Australia

Barbel Koribalski

Australia Telescope National Facility/Commonwealth Scientific and Industrial Research Organisation

Snezana Stanimirovic

University of California, Berkeley

Follow this and additional works at: https://digitalcommons.carleton.edu/phys_faculty



Part of the [Physics Commons](#)

Recommended Citation

Weisberg, Joel M., Simon Johnston, Barbel Koribalski, and Snezana Stanimirovic., "Discovery of pulsed OH emission stimulated by a pulsar". *Science*, vol. 309, no. , 2005. Available at: <https://doi.org/10.1126/science.1112494>. . [Online]. Accessed via Faculty Work. Physics and Astronomy. *Carleton Digital Commons*. https://digitalcommons.carleton.edu/phys_faculty/7

The definitive version is available at <https://doi.org/10.1126/science.1112494>

This Article is brought to you for free and open access by the Physics and Astronomy at Carleton Digital Commons. It has been accepted for inclusion in Faculty Work by an authorized administrator of Carleton Digital Commons. For more information, please contact digitalcommons.group@carleton.edu.

This copy is for your personal, non-commercial use only.

If you wish to distribute this article to others, you can order high-quality copies for your colleagues, clients, or customers by [clicking here](#).

Permission to republish or repurpose articles or portions of articles can be obtained by following the guidelines [here](#).

The following resources related to this article are available online at www.sciencemag.org (this information is current as of June 1, 2011):

Updated information and services, including high-resolution figures, can be found in the online version of this article at:

<http://www.sciencemag.org/content/309/5731/106.full.html>

Supporting Online Material can be found at:

<http://www.sciencemag.org/content/suppl/2005/06/30/1112494.DC1.html>

A list of selected additional articles on the Science Web sites **related to this article** can be found at:

<http://www.sciencemag.org/content/309/5731/106.full.html#related>

This article has been **cited by** 9 article(s) on the ISI Web of Science

This article has been **cited by** 1 articles hosted by HighWire Press; see:

<http://www.sciencemag.org/content/309/5731/106.full.html#related-urls>

This article appears in the following **subject collections**:

Astronomy

<http://www.sciencemag.org/cgi/collection/astronomy>

Discovery of Pulsed OH Maser Emission Stimulated by a Pulsar

Joel M. Weisberg,^{1,2,3*} Simon Johnston,^{2,1} Bärbel Koribalski,¹ Snezana Stanimirović⁴

Stimulated emission of radiation has not been directly observed in astrophysical situations up to this time. Here we demonstrate that photons from pulsar B1641–45 stimulate pulses of excess 1720-megahertz line emission in an interstellar hydroxyl (OH) cloud. As this stimulated emission is driven by the pulsar, it varies on a few-millisecond time scale, which is orders of magnitude shorter than the quickest OH maser variations previously detected. Our 1612-megahertz spectra are inverted copies of the 1720-megahertz spectra. This “conjugate line” phenomenon enables us to constrain the properties of the interstellar OH line-producing gas. We also show that pulsar signals undergo significantly deeper OH absorption than do other background sources, which confirms earlier tentative findings that OH clouds are clumpier on small scales than are neutral hydrogen clouds.

Pulsars are outstanding tools for the study of the interstellar medium (ISM). Their pulsed signals undergo a variety of modifications as they propagate through the ISM, revealing extensive information about the global distribution and physical properties of the intervening material. The tiny sizes of pulsars ensure that their signals probe very small transverse scales in the ISM (1, 2). Another virtue of pulsar ISM measurements is that the pulsars cycle rapidly on and off, so that observations may be made contemporaneously in both the presence and absence of the pulse, and the properties of the medium can be precisely compared in these two states. For example, the comparison of neutral hydrogen (HI) spectra acquired during and between pulses leads to pulsar absorption spectra that can be used for determinations of kinematic distance and interstellar electron density (3–5). Recently, Stanimirović *et al.* (6) extended the pulsar spectral technique to the OH molecule with the first successful OH absorption measurements toward pulsar PSR B1849+00. We expanded OH spectral measurements to 18 additional pulsars, chosen because they are relatively bright and lie in the inner Galaxy near the galactic plane. One of them, B1641–45 = PSR J1644–4559, not only exhibits intervening OH absorption at

1612, 1665, and 1667 MHz, but also shows interstellar stimulated emission at 1720 MHz.

The widths and strengths of spectral lines from some interstellar molecules provide abundant indirect evidence for stimulated emission processes; soon after the discovery of interstellar OH in the 1960s, it was recognized that maser processes must be involved (7–9). Beam-switched OH measurements toward the radio galaxy 3C123 have also demonstrated that a background source can stimulate emission in interstellar OH (10). The pulsed 1720-MHz maser detection reported here represents direct astronomical observation of the process of the radiative stimulation of emission. The broadband pulsar spectrum exhibits excess line emission at 1720 MHz as the pulsar’s photons stimulate the creation of additional photons in an intervening OH cloud. This excess emission switches on and off with the pulsar, clearly demonstrating its stimulated nature. We analyzed these pulsar absorption and stimulated emission observations, and compare them here with similar measurements in nonpulsar observations to study the physical properties of the intervening medium.

A pulsar-binning spectrometer was used to ultimately create two separate spectra: a “pulsar” spectrum and a “pulsar-off” spectrum (11). The pulsar spectrum represents the signal of the pulsar alone, as absorbed or amplified by intervening OH. In contrast, the pulsar-off spectrum is sensitive to OH emission or absorption occurring anywhere within the telescope beam. The main OH lines at 1665 and 1667 MHz were simultaneously observed in the 4-MHz bandpass with several-hour integrations for each of the 18 pulsars in our sample. (See Table 1 for total integration times and for

1 σ optical depth uncertainties in the Hanning smoothed pulsar spectra.) After our success in detecting absorption in the 1665- and 1667-MHz pulsar spectra of PSR B1641–45, we also measured the satellite (1612- and 1720-MHz) lines toward the pulsar.

In order to calculate the optical depth τ of absorption or stimulated emission, we considered the defining equation for optical depth, $I/I_0 = e^{-\tau}$, where I_0 is the original intensity measured offline and I is the intensity after traversal through optical depth τ of material. The differencing procedure leading to the pulsar spectrum automatically eliminates all nonpulsar signals and yields the spectrum in units of $(I/I_0)_{\text{PSR}}$, so it is straightforward to calibrate the pulsar spectrum in terms of τ . It is not so simple to determine optical depths in the pulsar-off spectra for several reasons. First, it is not clear whether the background emission and foreground absorption/amplification regions subtend the same solid angle. It is probably reasonable to assume in our case that the background fills the telescope beam, because its predominant source is the smoothly distributed galactic nonthermal emission, but the size of the foreground clouds is unknown from our measurements. Consequently, in the absence of better information, we will assume that both foreground and background fill the beam, so that $I/I_0 = T/T_0$, where T is the original brightness temperature (measured offline) and T_0 is the brightness temperature after traversal through the materi-

Table 1. Integration times and pulsar spectrum noise fluctuations.

PSR J	PSR B	Freq (MHz)	t_{tot} (hour)	σ_{τ}^* (pulsar spectrum)
0742-2822	0740-28	1665/7	3	0.1
0835-4510	0833-45	1665/7	2	0.1
0837-4135	0835-41	1665/7	4	0.07
0908-4913	0906-49	1665/7	4	0.1
1056-6258	1054-62	1665/7	2	0.1
1057-5226	1055-52	1665/7	1	0.1
1157-6224	1154-62	1665/7	2	0.3
1243-6423	1240-64	1665/7	2	0.1
1326-5859	1323-58	1665/7	2	0.1
1327-6222	1323-62	1665/7	2	0.1
1600-5044	1557-50	1665/7	7	0.1
1605-5257	1601-52	1665/7	1	0.2
1644-4559	1641-45	1665/7	5	0.01
1644-4559	1641-45	1720	5	0.01
1644-4559	1641-45	1612	4	0.01
1745-3040	1742-30	1665/7	5	0.2
1752-2806	1749-28	1665/7	4	0.05
1803-2137	1800-21	1665/7	5	0.3
1825-0935	1822-09	1665/7	1	0.3
1829-1751	1826-17	1665/7	2	0.3

*The quantity σ_{τ} (pulsar spectrum) is the optical depth standard deviation in the Hanning smoothed pulsar spectrum, which includes the effects of radiometer and sky noise, and in some cases, interstellar scintillation.

¹Australia Telescope National Facility/Commonwealth Scientific and Industrial Research Organisation, Post Office Box 76, Epping, NSW 1710, Australia.

²School of Physics, University of Sydney, Sydney, NSW 2006, Australia. ³Department of Physics and Astronomy, Carleton College, Northfield, MN 55057, USA. ⁴Department of Astronomy, University of California, Berkeley, CA 94720, USA.

*To whom correspondence should be addressed. E-mail: jweisber@carleton.edu

al (see below). However, another difficulty is that the observed continuum is emitted throughout the line of sight across the Galaxy, whereas the definition of τ requires that T_o be only that portion emitted beyond the cloud contributing to optical depth. In order to estimate the fraction of the continuum $f(d)$ contributing to T_o as a function of distance d , we synthesized a model of the continuum emission $\epsilon(s)$ as a function of distance s along the line of sight, consisting of galactic synchrotron (12), ionized hydrogen regions, and the 2.7-K cosmic background radiation. We then integrated this model along the appropriate (background) part of the line of sight and normalized the result by the total emission along the line of sight

$$f(d) = \frac{\epsilon_{\text{background}}}{\epsilon_{\text{tot}}} = \frac{\int_d^\infty \epsilon(s) ds}{\int_0^\infty \epsilon(s) ds} \quad (1)$$

Then $T_o(d) = T_{\text{bo}} f(d)$, where T_{bo} is the brightness temperature offline, determined as described in (11). Combining all the above results for pulsar-off spectra, we find that $\tau = -\ln(I/I_o) = -[T/T_o(d)] = -\ln[T/f(d)T_{\text{bo}}(d)]$. Distance was then mapped to radial velocity of the spectra with a galactic rotation model (13).

Figure 1 displays the 1720-MHz spectra toward PSR B1641–45, which directly demonstrate the process of stimulated emission. The pulsar-off spectrum (Fig. 1A, bottom), which was acquired in the interval between pulses, shows both emission and absorption against other background source(s) lying within the 13-arc min telescope beam. The pulsar-on spectrum (Fig. 1A, top) appears to zeroth order to be merely a copy of the pulsar-off spectrum, shifted upward by a constant equal to the broadband pulsar signal strength. However, when these two spectra are carefully differenced (11) to create the pulsar spectrum (Fig. 1B), it is clear that there is excess signal at velocity (v) ~ -45 km/s, where the broadband pulsar signal has been amplified by stimulated emission. It has long been thought that stimulated emission plays an important role in astrophysical OH line radiation. For example, line temperatures are frequently far in excess of those inferred from (assumed thermal) line widths (7–9). However, our measurements directly demonstrate the stimulated amplification of a signal propagating through the ISM, in that the amplification is directly observable as the pulsar cycles on and off during its 455-ms rotational period. As the stimulated emission switches on and off synchronously with the pulsar pulse, our 14-ms time resolution [1/32nd of the pulse period

(14)] places a very short upper limit on its duration. Because the shortest intrinsic fluctuation time scale previously reported was ~ 1000 s (15), these variations are by far the quickest observed in any interstellar maser.

Two conditions must be satisfied in order for stimulated emission to occur. First, the populations at the relevant levels must be inverted or pumped by some process. Second, appropriate photons should be available to stimulate the emission from the upper overpopulated level. In our case, the level inversion is accomplished locally in the OH cloud by a low-energy radiative or collisional process, whereas the stimulating photons are provided by the pulsar.

The pulsed maser line optical depth $\tau \sim -0.05$, which implies that approximately five excess line photons are stimulated in the cloud for every hundred passing through it. Because the maser is unsaturated with a gain of only 1.05, we expect that the full width at half maximum (FWHM) of the line should be very similar to the expected thermal line width, which is about 0.5 to 0.7 km/s for gas with kinetic temperature of 100 to 200 K. For example, a typical FWHM of 0.5 km/s was found in a large survey of 1720-MHz masers in star-forming regions (16). The FWHM we measure is about 2 km/s, which is slightly wider and suggests that we are most likely seeing a blend of several maser spots along the line of sight.

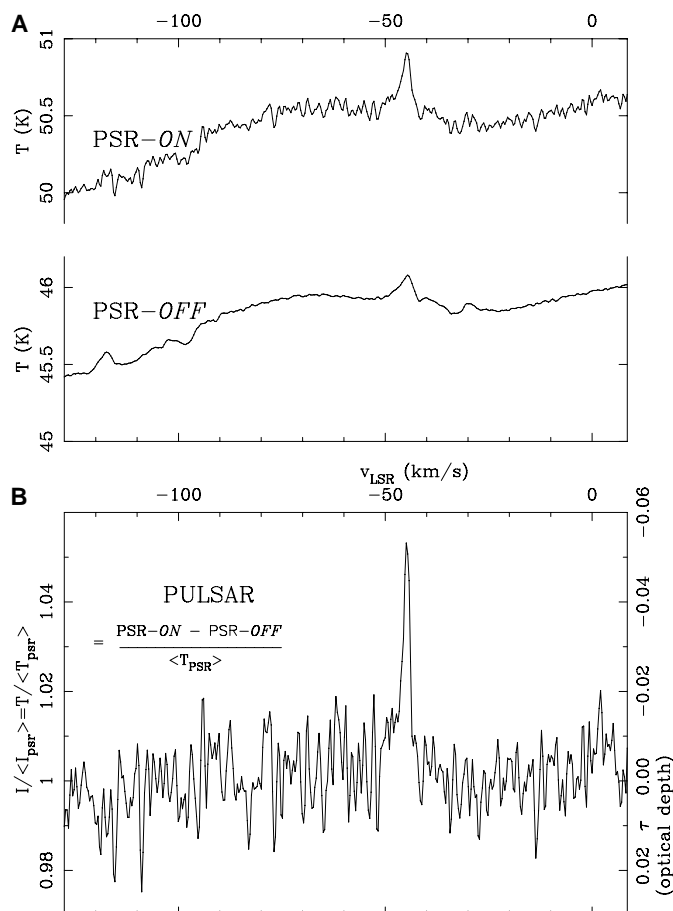
It has been suggested (17) that extraterrestrial civilizations could use interstellar masers to amplify their radio transmissions. We have demonstrated here that such a process could sustain modulation down to millisecond time scales, but of course the gain of this particular maser is too small to provide significant amplification of an extraterrestrial intelligent signal.

PSR B1641–45 = J1644–4559 lies in a well-studied (18–22) region of the inner Galaxy near the galactic plane, at galactic longitude l and latitude b (l, b) = (339.2°, –0.2°). We were able to construct a schematic map of the ISM along the line of sight by combining our observations with earlier ones (Fig. 2).

On the basis of kinematic analysis of HI absorption spectra (23), the pulsar is placed 4.6 kpc along the line of sight. Two ionized hydrogen (HII) regions lie in this direction, with galactic coordinates and recombination line velocities with respect to the local standard of rest (LSR), v_{LSR} (19, 20) of (l, b, v_{LSR}) = (339.1°, –0.2°, –120 km/s) and (339.1°, –0.4°, –37 km/s). With the rotation curve of (13), our kinematic analysis of the recombination line measurements places G339.1–0.2 beyond the pulsar at a geocentric distance $d \sim 6.7$ kpc and places G339.1–0.4 closer than the pulsar at $d \sim 3.3$ kpc.

Figure 3 displays spectra at frequencies of the four ground-rotational state, 18-cm

Fig. 1. Stimulated amplification of the PSR B1641–45 signal in an interstellar OH cloud at 1720 MHz. (A) The pulsar-on (top) spectrum, acquired during the pulsar pulse, and (bottom) the pulsar-off spectrum, gathered in the interval between pulses. The two spectra exhibit both emission and absorption against other (nonpulsar) background source(s) lying within the 13-arc min telescope beam, whereas the pulsar-on spectrum additionally contains the pulsar signal. (B) The pulsar spectrum, the difference of pulsar-on and pulsar-off spectra, illustrating the pulsar signal alone as absorbed (or in this case, amplified) by intervening OH. The spike in this spectrum at $v_{\text{LSR}} \sim -45$ km/s results from excess emission in an OH cloud, stimulated by pulsar photons.



OH lines toward PSR B1641–45. There is a strong spectral line at $v_{\text{LSR}} \sim -45$ km/s in all of our OH spectra, both pulsar-off and pulsar spectra. The line is in absorption at 1612, 1667, and 1665 MHz and in emission at 1720 MHz (the latter being the pulsed maser emission discussed above). Because it is visible in the pulsar spectra (Fig. 3, right column), this line must arise between the pulsar and the observer. It probably originates in OH gas associated with or near G339.1-0.4, because the velocities are similar. However, pervasive extended regions of 1720-MHz emission have been found in the inner galactic plane (24, 25), including a $>1^\circ$ -long filament crossing near the pulsar line of sight with $v_{\text{LSR}} \sim -40$ km/s. Because our 1720-MHz pulsar-off spectral line at -45 km/s has strength and width similar to those of the extended OH gas (although the velocities are somewhat discrepant), it is possible that it originates from this extended OH region rather than from the HII region G339.1-0.4.

The -45 -km/s emission and absorption features show evidence for departures from local thermodynamic equilibrium (LTE). The pulsar-off spectra typically have FWHM of 2 to 3 km/s, which is a few times wider than what is expected for thermally broadened line profiles at a typical kinetic temperature of about 100 K. The peak optical depths are very similar at 1667 and 1665 MHz ($\tau \sim 0.03$), whereas in the LTE case, their ratio would be 9/5, respectively. In addition, the 1612 MHz lines are inverted with respect to 1720 MHz.

We see another OH line at $v_{\text{LSR}} \sim -30$ km/s in most of the eight spectra toward PSR B1641–45 shown in Fig. 3, including the 1665- and 1667-MHz pulsar spectra. This line must therefore also originate in gas nearer to us than the pulsar, probably associated with or near G339.1-0.4. The lines are seen in absorption in pulsar spectra and primarily in emission in pulsar-off spectra.

Finally, all pulsar-off spectra exhibit line(s) at $v_{\text{LSR}} \sim -100$ to -120 km/s, which are not seen in the pulsar spectra. Consequently, they must originate in gas beyond the pulsar, probably associated with or near G339.1-0.2.

Each 1720-MHz spectrum (Fig. 3, top row) is an inverted copy of the 1612-MHz spectrum (Fig. 3, second row). This phenomenon, called conjugate line behavior, occurs because the initial states of both transitions are overpopulated by an identical process (8, 26–28). For our predominantly observed conjugate state, which has 1720-MHz stimulated emission and 1612-MHz stimulated absorption, the process begins in a region with $T \sim 100$ K and OH number density $n_{\text{OH}} \sim 10^5 \text{ cm}^{-3}$ with the collisional excitation of the molecule to a higher

rotational state at energy $E = 1.66 \times 10^{-14}$ ergs above ground level, after which it can radiatively decay with equal probability (if the transition is optically thick) to overpopulate either the upper level of the 1720-MHz transition or the lower level of the 1612-MHz transition. The 1612-MHz stimulated emission and conjugate 1720-MHz stimulated absorption, which we observed more rarely, result from a similar process that overpopulates the opposite 18-cm levels via an intermediate excited rotational level at $E = 2.5 \times 10^{-14}$ ergs above the ground level.

The predominant conjugate configuration becomes optically thick to far-infrared photons for OH column densities N_{OH} per velocity interval $N_{\text{OH}}/\Delta v > 10^{14} \text{ s km}^{-1} \text{ cm}^{-2}$, whereas the inverse configuration becomes optically thick and then dominates at $N_{\text{OH}}/\Delta v > 10^{15} \text{ s km}^{-1} \text{ cm}^{-2}$. Hence our predominant conjugate configuration (including the 1720-MHz pulsar-stimulated emission and the pulsar-off emission at $v \sim -120$ km/s) originates in clouds with specific column densities between these two limits, whereas the rarer opposite configuration (e.g., pulsar-off 1720-MHz absorption at $v \sim -100$ km/s) originates in a column whose density is above the upper limit. Then the occasionally observed adjacent emission and absorption features that are conjugate at the two frequencies (e.g., the pulsar-off spectra at $v \sim -32$ km/s) suggest a density gradient in the cloud (28), with specific column densities crossing $10^{15} \text{ s km}^{-1} \text{ cm}^{-2}$ at the transition.

We compared the lines observed in the pulsar and pulsar-off spectra, because all the

lines were acquired at the same time, with the telescope pointing in exactly the same direction. To facilitate the comparison, optical depth scales on the right side of all eight spectra in Fig. 3 are identical. The lines where $v \sim -45$ km/s exhibit markedly stronger ($|\tau| \sim 2$ to 3 times larger) absorption and stimulated emission in pulsar spectra (Fig. 3, right column) than those in the corresponding pulsar-off spectra (Fig. 3, left column). The discrepancy at $v \sim -32$ km/s is even stronger; absorption in pulsar spectra at 1665 and 1667 MHz is absent or replaced by weak emission in pulsar-off spectra (29). The only other successful pulsar OH absorption experiment (6) also found stronger absorption in the pulsar spectra than in the pulsar-off spectra.

The widths of the lines are narrower in our pulsar spectra than in pulsar-off spectra at 1720 and 1612 MHz, but similar at 1667 and 1665 MHz. The earlier results (6) exhibited narrower lines in the pulsar spectra than in the pulsar-off spectra at 1667 and 1665 MHz.

Our observations strengthen the earlier interpretation that the needle-thin interstellar column sampled by the pulsar signal interacts with a substantially different sample of the medium than does the pulsar-off column, which represents the average of all interactions across the 13-arc min telescope beam. Presumably the pulsar signal is encountering small and dense OH cloudlets, whose properties are diluted in the beam-averaged pulsar-off spectrum. This behavior differs markedly from HI, where the statistics show no dependence on the angular cross-sections of absorbing columns across a tremendous range of

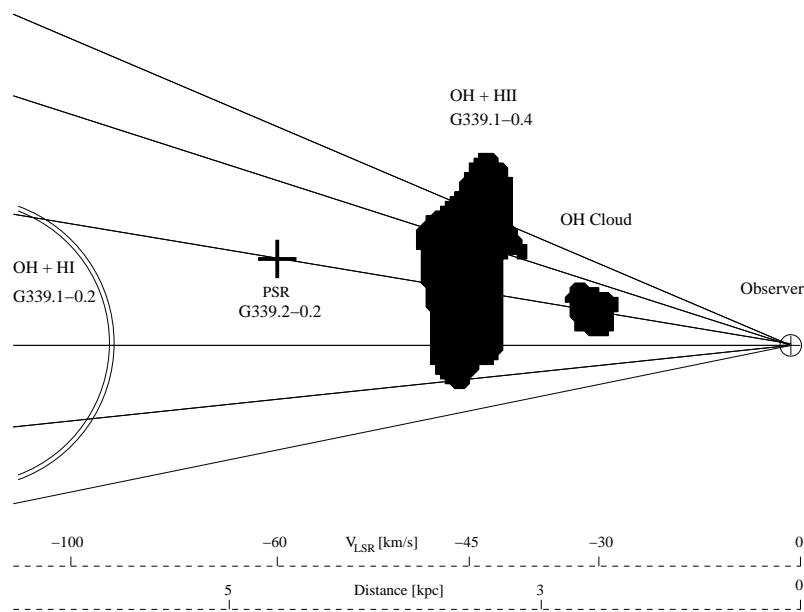


Fig. 2. A schematic model of the ISM toward PSR B1641–45. The ionized region velocities are from (19, 20), the OH velocities are from our current work, and the limiting pulsar HI absorption velocities are from (23). The kinematic velocity-to-distance conversion uses the rotation curve of (13). The lines represent various lines of sight within the 13-arc min telescope beam. The vertical scale has been enlarged for clarity.

solid angles (30, 31). Molecular gas is known to be more clumped than neutral gas, at least on larger scales.

If the difference in OH optical depths indeed results from clumping, we would expect that other pulsar lines of sight would pierce regions devoid of cloudlets and show shallower optical depths than pulsar-off measurements. One might ask why there are no such complementary results. Unfortunately, an

observational selection effect prevents success in such observations, because we do not have sufficient sensitivity on any other pulsar lines of sight (Table 1) to test this hypothesis.

An earlier paper (32) reported broad ($\Delta v > 10$ km/s) and deep ($\tau > 0.5$) OH absorption at 1667 MHz in the spectrum of PSR B1749–28. We have adequate sensitivity to detect such a line (Table 1), but we do not confirm the result. All other OH lines detected in pulsar spectra

are much narrower than the previously claimed detection in PSR B1749–28.

We have searched for OH absorption and stimulated emission in the spectrum of 18 pulsars. One pulsar, B1641–45, exhibits absorption or stimulated emission in pulsar spectra at each of the four 18-cm line frequencies. No absorption or stimulated emission was detected in the others, including one in which OH absorption had previously been reported (B1749–28). A variety of results are drawn from the B1641–45 spectra. The pulsed maser line, with $\tau \sim -0.05$, represents the first direct detection of interstellar stimulated emission. The OH and HII concentrations are mapped along the line of sight to the pulsar, and they are found to be associated kinematically and probably spatially. Analysis of the lines provides insight into the OH density, temperature, and excitation. Finally, the relative depths of lines in pulsar spectra and pulsar-off spectra suggest that the OH gas is highly clumped.

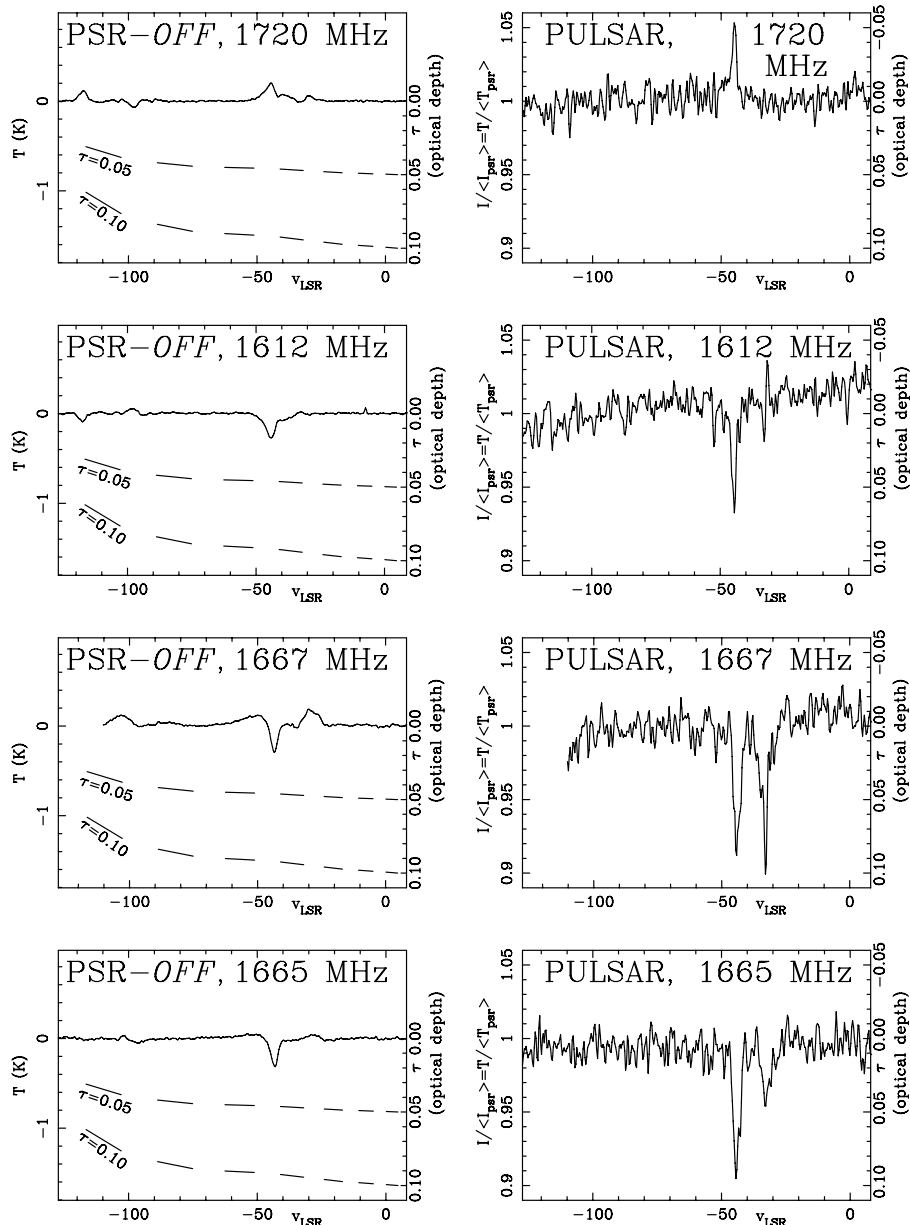


Fig. 3. Spectra of the four 18-cm ground-state rotational transitions of OH toward PSR B1641–45. The left column displays the four pulsar-off spectra, which are sensitive to all emission and absorption in the 13-arc min telescope beam when the pulsar is switched off. The right column shows the four pulsar spectra, which exhibit the absorption or stimulated emission of the pulsar signal alone. The righthand ordinate on each panel is optical depth τ ; all eight spectra are plotted with the same optical depth scale. All pulsar-off spectral features are significantly shallower (i.e., have smaller optical depths) than their analogs in the pulsar spectra. In the pulsar-off spectra, the sloping lines of constant optical depth result from changes in the ratio of background to total continuum along the line of sight (see discussion accompanying Eq. 1). Low-order sinusoids were fitted to and removed from the pulsar-off baselines in order to flatten them.

References and Notes

1. J. M. Cordes, J. M. Weisberg, V. Boriakoff, *Astrophys. J.* **288**, 221 (1985).
2. S. Johnston, L. Nicastro, B. Koribalski, *Mon. Not. R. Astron. Soc.* **297**, 108 (1998).
3. B. Koribalski, S. Johnston, J. M. Weisberg, W. Wilson, *Astrophys. J.* **441**, 756 (1995).
4. J. M. Weisberg, M. H. Siegel, D. A. Frail, S. Johnston, *Astrophys. J.* **447**, 204 (1995).
5. S. Johnston, B. Koribalski, J. M. Weisberg, W. Wilson, *Mon. Not. R. Astron. Soc.* **322**, 715 (2001).
6. S. Stanimirović et al., *Astrophys. J.* **592**, 953 (2003).
7. A. H. Cook, *Celestial Masers* (Cambridge Univ. Press, Cambridge, 1977).
8. M. Elitzur, *Astronomical Masers* (Kluwer, Dordrecht, 1992).
9. M. Claussen, *Science* **306**, 235 (2004).
10. N. Q. Rieu et al., *Astron. Astrophys.* **46**, 413 (1976).
11. Materials and methods are available as supporting material on Science Online.
12. K. Beuermann, G. Kanbach, E. M. Berkhuijsen, *Astron. Astrophys.* **153**, 17 (1985).
13. M. Fich, L. Blitz, A. A. Stark, *Astrophys. J.* **342**, 272 (1989).
14. The pulsar-binning spectrometer was adjusted so that the pulsar pulse fell entirely within one of the 32 phase bins (17). Consequently, no information on possible shorter-time scale phenomena is available.
15. A. W. Clegg, J. M. Cordes, *Astrophys. J.* **374**, 150 (1991).
16. J. L. Caswell, *Mon. Not. R. Astron. Soc.* **349**, 99 (2004).
17. J. Cordes, *Astron. Soc. Pacific Conf. Series* **47**, 257 (1993).
18. R. N. Manchester, U. Mebold, *Astron. Astrophys.* **59**, 401 (1977).
19. P. A. Shaver, R. X. McGee, L. M. Newton, A. C. Danks, S. R. Pottasch, *Mon. Not. R. Astron. Soc.* **204**, 53 (1983).
20. J. L. Caswell, R. F. Haynes, *Astron. Astrophys.* **171**, 261 (1987).
21. J. C. Cersosimo, *Astrophys. J.* **349**, 67 (1990).
22. N. M. McClure-Griffiths et al., *Astrophys. J. Suppl.* **158**, 178 (2005).
23. D. A. Frail, J. M. Weisberg, *Astron. J.* **100**, 743 (1990).
24. R. F. Haynes, J. L. Caswell, *Mon. Not. R. Astron. Soc.* **178**, 219 (1977).
25. B. E. Turner, *Astrophys. J.* **255**, L33 (1982).
26. H. J. van Langevelde, E. F. van Dishoeck, M. N. Sevenster, F. P. Israel, *Astrophys. J.* **448**, L123 (1995).
27. P. Lockett, E. Gauthier, M. Elitzur, *Astrophys. J.* **511**, 235 (1999).
28. K. J. Brooks, J. B. Whiteoak, *Mon. Not. R. Astron. Soc.* **320**, 465 (2001).
29. The $v \sim -100$ km/s lines in the pulsar-off spectra cannot have analogs in the pulsar spectra because they originate in gas beyond the pulsar.
30. J. M. Dickey, J. M. Weisberg, J. M. Rankin, V. Boriakoff, *Astron. Astrophys.* **101**, 332 (1981).

31. H. E. Payne, Y. Terzian, E. E. Salpeter, *Astrophys. J. Suppl. Ser.* **48**, 199 (1982).
32. V. I. Slysh, *Astronomicheskii Cirkular* **731**, 1 (1972).
33. We thank J. Reynolds and W. Wilson for assistance with the gated correlator configuration, K. Wells and K. Willett for help with the observations, and R. Norris and J. Caswell for providing useful suggestions. J.M.W. gratefully acknowledges financial support from NSF

grant AST 0406832, the Australia Telescope National Facility, and the School of Physics of the University of Sydney. S.S. acknowledges support from NSF grants AST 0097417 and AST 9981308. The Parkes telescope is part of the Australia Telescope funded by the Commonwealth of Australia for operation as a National Facility managed by the Commonwealth Scientific and Industrial Research Organisation.

Supporting Online Material
www.sciencemag.org/cgi/content/full/1112494/DC1
 Materials and Methods

21 March 2005; accepted 10 May 2005
 Published online 26 May 2005;
 10.1126/science.1112494
 Include this information when citing this paper.

A High-Pressure Structure in Curium Linked to Magnetism

S. Heathman,^{1*} R. G. Haire,² T. Le Bihan,^{3†} A. Lindbaum,⁴ M. Idiri,¹
 P. Normile,¹ S. Li,^{5,6} R. Ahuja,^{5,6} B. Johansson,^{5,6} G. H. Lander¹

Curium lies at the center of the actinide series and has a half-filled shell with seven *5f* electrons spatially residing inside its radon core. As a function of pressure, curium exhibits five different crystallographic phases up to 100 gigapascals, of which all but one are also found in the preceding element, americium. We describe here a structure in curium, Cm III, with monoclinic symmetry, space group *C2/c*, found at intermediate pressures (between 37 and 56 gigapascals). *Ab initio* electronic structure calculations agree with the observed sequence of structures and establish that it is the spin polarization of curium's *5f* electrons that stabilizes Cm III. The results reveal that curium is one of a few elements that has a lattice structure stabilized by magnetism.

The contribution of various factors in the electronic structure of a material to the bonding in its solid phase is at the heart of materials science and is a subject of extensive experimental and theoretical interest. It is well known that, when approaching the center of the actinide (*5f*) series of elements, a marked change occurs in the elemental volumes. The atomic volume of americium (Am) is almost 50% larger than that for the preceding element plutonium (Pu) (Fig. 1). The lighter actinides (Pa to Pu) have smaller atomic volumes and itinerant *5f* states that participate in the (metallic) bonding and thus contribute to the cohesive properties of the solid. However, the *5f* states are also capable of spin-polarization and hence magnetism. When the *5f* bands are broad, as in the itinerant metals (Pa to Pu), there is an absence

of magnetic correlations (1, 2). However, for heavier actinide elements (Am and beyond), there is no *5f* bonding, and magnetic correlations give rise to local moments, as found in the analogous *4f* elements. Of particular interest with these heavier actinides is whether applied pressure can bring about the delocalization (a change of character from localized to itinerant) of their *5f* electrons, and, if so, what are the consequent crystallographic, electronic, and magnetic structures?

In the periodic table, iron and cobalt are unique in the sense that the magnetic interactions between *d* electron states determine their crystal structures (3–5). Given that the magnetic correlations are between *f* electron states in the actinides, we may ask whether such magnetic interactions can influence the sequence of crystal structures.

There are fundamental differences in the pressure-volume relationships of the light (6, 7) and heavy actinide metals (Fig. 1). Under compression, the relative volume changes with pressure for α -uranium (the room-temperature-stable form of uranium metal) (7) are clearly different from those for either Am or curium (Cm). We have investigated in detail the case of Am (8, 9), where four crystal structures are found to exist between ambient pressure and 100 GPa. The delocalization of the *5f* electrons of Am by pressure occurs in two stages, with the progressive formation of two lower symmetry structures, a face-centered orthorhombic Am III and a primitive orthorhombic structure, Am IV; the transition to each is accompanied by an abrupt decrease in the relative atomic volume. The formation of the Am IV structure

(space group, *Pnma*), which was subsequently confirmed by theory (10), is now recognized as an important high-pressure structure for *f* electron metals.

In Cm, the *5f*⁷ half-filled orbital provides a stabilizing effect. Consequently, forcing its *5f* electrons to participate in its bonding requires higher pressures than in the case of Am. At ambient pressure, only the *6d 7s* states of these elements are involved in their metallic bonding (2). With the application of pressure, the double hexagonal close packed (dhcp) form of Cm (*P6₃/mmc*, Cm I) converts to a face-centered cubic (fcc) structure (*Fm3m*, Cm II) at 17(2) GPa. This transformation requires little energy and reflects an increase in the *d* character of the bonding. There is a smooth transition between the Cm I and Cm II phases (Fig. 1), indicating that each phase has a comparable bulk modulus. This same transition occurs in Am, but at a lower pressure (6 GPa) (8, 9).

Previous work (11, 12) has identified the initial dhcp-fcc transition and also reported a phase transition above 40 GPa, but was unable to determine the correct structure. Given the pressure behavior of Am, one could have anticipated finding a structure similar to the Am III structure (*Fddd*) after the Cm II phase. However, our synchrotron radiation data show unambiguously that the Cm III phase is not *Fddd* as found for Am III. Before looking in detail at this Cm III phase, we will discuss the higher pressure phases of Cm.

Increasing the pressure above 56(4) GPa results in a third phase transition (Cm III to Cm IV), and this phase can indeed be identified with the *Fddd* structure as found for Am III. A smooth transition is observed between the Cm III and Cm IV phases. Above 95(5) GPa, the fourth phase transition (Cm IV to Cm V) is observed and yields a *Pnma* phase, which was previously identified for the Am IV structure. The *Fddd* to *Pnma* (Cm IV to Cm V) transition is accompanied by an ~11.7% volume collapse, whereas at the Cm II to Cm III transition, the collapse is ~4.5%. These abrupt volume changes signify the stepwise delocalization of the *5f* electrons and their subsequent participation in the metallic bonding. In Am, the total collapse of ~9% for two transitions is smaller than that for Cm, but in both elements the collapses occur in two stages. The appearance of the *Fddd* and *Pnma* forms for Am (8, 9) and Cm at higher pressures is a clear indication that the *5f* delocalization process favors these structures.

¹European Commission, Joint Research Centre, Institute for Transuranium Elements, Postfach 2340, D-76125, Karlsruhe, Germany. ²Oak Ridge National Laboratory (ORNL), Chemical Sciences Division, Office Box 2008, MS-6375, Oak Ridge, TN 37831, USA.

³European Synchrotron Radiation Facility (ESRF), Boite Postale 220, F-38043 Grenoble, France. ⁴Vienna University of Technology, Institute for Solid State Physics, Wiedner Hauptstrasse 8-10/138, A-1040, Vienna, Austria. ⁵Department of Physics, Uppsala University, Box 530, S-751 21 Uppsala, Sweden. ⁶Applied Materials Physics, Department of Materials Science and Engineering, Royal Institute of Technology, SE-100 44 Stockholm.

[†]Present address: Commissariat à l'Energie Atomique Valduc, Département de Recherches sur les Matériaux Nucléaires, Service Etudes de Métallurgie Physique, Laboratoire Etudes des Constantes Physiques, F-21120 Is-sur-Tille, France.

*To whom correspondence should be addressed.
 E-mail: heathman@itu.fzk.de